Resource

Cell Reports

Active Ribosome Profiling with RiboLace

Graphical Abstract

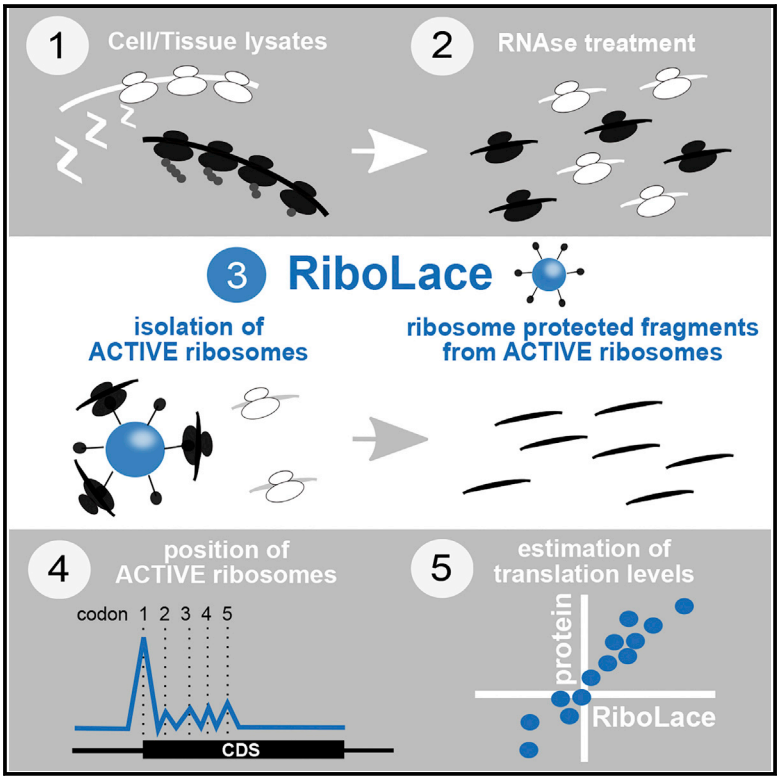

Highlights

- RiboLace isolates ribosomes in active translation by antibody-free and tag-free pull-down
- RiboLace works reliably with low amounts of input material *in vitro* and *in vivo*
- RiboLace provides positional data of active ribosomes with nucleotide resolution
- RiboLace estimates translation levels and predicts protein levels with accuracy

Authors

Massimiliano Clamer, Toma Tebaldi, Fabio Lauria, ..., Thomas H. Gillingwater, Alessandro Quattrone, Gabriella Viero

Correspondence

mclamer@immaginabiotech.com (M.C.), gabriella.viero@cnr.it (G.V.)

In Brief

Clamer et al. present RiboLace, a method for isolating active ribosomes and associated proteins, intact mRNAs, or ribosome-protected fragments. RiboLace accurately quantifies translation levels, providing positional data of active ribosomes with nucleotide resolution. Requiring lower input than current ribosome profiling protocols, RiboLace can be used with challenging biological samples.

Clamer et al., 2018, Cell Reports *25*, 1097–1108
October 23, 2018
https://doi.org/10.1016/j.celrep.2018.09.084

CellPress

Cell Reports
Resource

Active Ribosome Profiling with RiboLace

Massimiliano Clamer,[1,2,*] Toma Tebaldi,[1,8] Fabio Lauria,[3] Paola Bernabò,[3] Rodolfo F. Gómez-Biagi,[4] Marta Marchioretto,[3] Divya T. Kandala,[2] Luca Minati,[2] Elena Perenthaler,[3] Daniele Gubert,[3,5] Laura Pasquardini,[4] Graziano Guella,[6] Ewout J.N. Groen,[7] Thomas H. Gillingwater,[7] Alessandro Quattrone,[1] and Gabriella Viero[3,9,*]
[1]Centre for Integrative Biology, University of Trento, Via Sommarive, 9 Povo, Italy
[2]IMMAGINA Biotechnology s.r.l., Via alla cascata 56/c, Povo, Italy
[3]Institute of Biophysics, CNR Unit at Trento, Via Sommarive, 18 Povo, Italy
[4]Fondazione Bruno Kessler-LaBSSAH, Via Sommarive, 18 Povo, Trento, Italy
[5]Department of Information Engineering and Computer Science, University of Trento, Povo, Italy
[6]Department of Physics, University of Trento, Povo, Italy
[7]Edinburgh Medical School: Biomedical Sciences, University of Edinburgh, Edinburgh, UK
[8]Present address: Yale Cancer Center, Yale University School of Medicine, New Haven, CT 06520, USA
[9]Lead Contact
*Correspondence: mclamer@immaginabiotech.com (M.C.), gabriella.viero@cnr.it (G.V.)
https://doi.org/10.1016/j.celrep.2018.09.084

SUMMARY

Ribosome profiling, or Ribo-seq, is based on large-scale sequencing of RNA fragments protected from nuclease digestion by ribosomes. Thanks to its unique ability to provide positional information about ribosomes flowing along transcripts, this method can be used to shed light on mechanistic aspects of translation. However, current Ribo-seq approaches lack the ability to distinguish between fragments protected by either ribosomes in active translation or inactive ribosomes. To overcome this possible limitation, we developed RiboLace, a method based on an original puromycin-containing molecule capable of isolating active ribosomes by means of an antibody-free and tag-free pull-down approach. RiboLace is fast, works reliably with low amounts of input material, and can be easily and rapidly applied both *in vitro* and *in vivo*, thereby generating a global snapshot of active ribosome footprints at single nucleotide resolution.

INTRODUCTION

The process of protein synthesis is a core regulator of numerous critical physiological pathways ranging from cell growth (Goyer et al., 1993) and development (Kondrashov et al., 2011; Xue et al., 2015) to immune response (Piccirillo et al., 2014). Local protein synthesis in neurons (Jung et al., 2014) also plays fundamental roles in memory formation (Fioriti et al., 2015; Kandel et al., 2014; Martin et al., 1997) and synaptic plasticity (McCamphill et al., 2015). Hence, dysregulation of translation is a major driver of important pathologies such as cancer (Bhat et al., 2015; Topisirovic and Sonenberg, 2015) and neurodegenerative diseases (Bernabò et al., 2017; Darnell et al., 2011).

During the last few years, methodological approaches such as ribosome profiling (Ribo-seq) (Ingolia et al., 2009) have contributed considerable insights into the translation process. Ribo-seq has been largely used to identify translated RNAs (both coding and, unexpectedly, non-coding), map upstream open reading frames (ORFs), and estimate translation levels in different biological conditions. Ribo-seq has been used to estimate translation efficiencies and "protein synthesis levels" (Ingolia et al., 2014; Li et al., 2014) in a variety of organisms, from prokaryotes (Li et al., 2014) to yeast (Ingolia et al., 2009), *Caenorhabditis elegans* (Stadler et al., 2012), zebrafish (Bazzini et al., 2014; Chew et al., 2013), plants (Juntawong et al., 2014), mouse (Ingolia et al., 2011), and human (Fritsch et al., 2012; Lee et al., 2012; Liu et al., 2013).

Despite its unquestionable discrimination power and wide applicability, Ribo-seq still faces a number of challenges and presents some limitations. For example, translationally inactive mRNAs can be sequestered into ribonucleoprotein particles (mRNPs) and stalled or paused in polysomes as a consequence of physiological surveillance mechanisms, stress stimuli, and regulatory mechanisms (Yordanova et al., 2018). The contribution of these phenomena in multicellular organisms is particularly important in specific tissues, and it has been shown to occur especially in neurons (Chapman and Walter, 1997; Darnell et al., 2011; Doma and Parker, 2006; Graber et al., 2013; Higashi et al., 2013). As such, while inactive ribosomes unbound to transcripts do not present a problem, Ribo-seq does not necessarily discriminate "authentic" protected footprints of translating polysomes from RNA fragments protected by inactive or stalled ribosomes, leading to possible misinterpretations of translation occupancy profiles. Therefore, to generate optimal insight into the translation process, Ribo-seq is still open to further optimization and refinements, incorporating aspects from the laboratory bench to data analysis (Aeschimann et al., 2015).

Here, we present RiboLace, a methodological approach to study active translation based on a newly developed reagent: a puromycin analog molecule. The aim of our study was to purify active ribosomes by immobilizing puromycylated ribosomes frozen on the transcript by the chain elongation inhibitor cycloheximide, which impedes the dissociation of ribosomal subunits (David et al., 2012). Our data show that RiboLace is useful for ribosome purification and the co-purification of associated proteins, intact mRNAs, and nuclease-protected footprints using

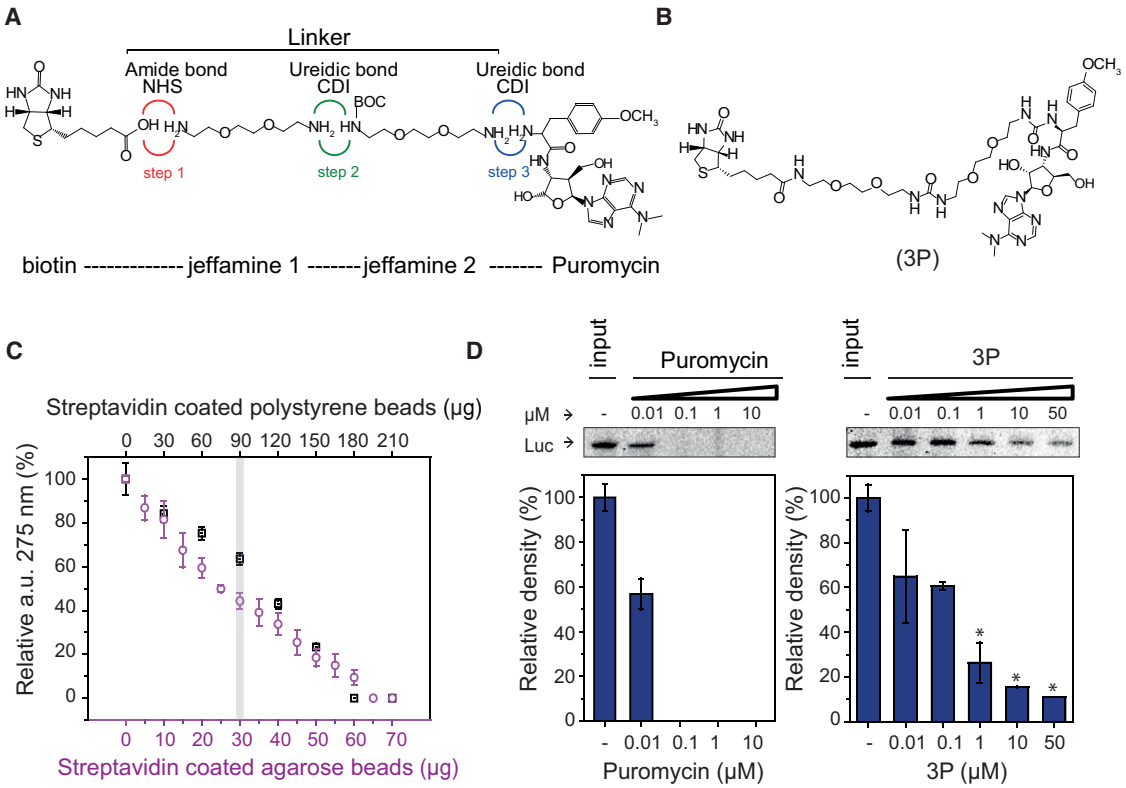

Figure 1. An Analog of Puromycin Inhibits Translation and Can Be Used for Functionalization of Agarose and Polystyrene Beads

(A) Schematic representation of the 3P structure. Biotin is the residue binding the surface; two 2,2′-ethylenedioxy-bis-ethylamine units form the "L" linker, and puromycin is the residue binding the ribosome. Steps 1–3 refer to the chemical synthesis procedure. CDI, *N*,*N*′-dicyclohexylcarbodiimide, jeffamine, 2,2′-ethylenedioxy-bis-ethylamine; NHS, *N*-hydroxysuccinimide.

(B) Chemical formula of the puromycin analog 3P.

(C) Depletion assay of 3P with streptavidin-coated agarose (purple) and polystyrene beads (black). Absorbance of the supernatant at 275 nm is measured after addition of streptavidin-coated magnetic beads to 100 pmol 3P. Data represent the mean of triplicate experiments. The gray bar marks the quantity of beads used in all of the experiments for each sample.

(D) Comparison between the efficiency of puromycin (left) and 3P (right) to inhibit the protein production of firefly luciferase. ε-Labeled biotinylated lysine-tRNA is used to monitor the protein production by SDS-PAGE (top). Histograms represent the change in protein production after the addition of different concentrations of puromycin or 3P with respect to the control. Error bars represent SDs calculated from triplicate experiments; n = 3; t test; *p < 0.05.

~40 times less material than classical ribosome profiling. RiboLace provides a valuable technique, with clear applications *in vitro* and *in vivo*.

RESULTS

Design and Synthesis of an Analog of Puromycin

Puromycin is an aminonucleoside antibiotic able to bind the ribosome and the nascent peptide chain, causing ribosome disassembly and disruption of protein synthesis (Nissen et al., 2000; Welch et al., 1995; Wilson, 2014; Yarmolinsky and Haba, 1959). It has been extensively used to quantify global protein synthesis, taking advantage of radioactive (Gambetti et al., 1972) and biotinylated molecules (Aviner et al., 2014) or anti-puromycin antibodies (Schmidt et al., 2009). Leveraging its ability to maintain contact with the ribosome (Kukhanova et al., 1979; Odom et al., 1990; Pestka et al., 1972; Schmeing et al., 2002), puromycin has also been used to covalently bind an mRNA to the corresponding protein during its synthesis (Biyani et al., 2006; Roberts and Szostak, 1997). In addition, puromycin can be modified to create cell-permeable analogs suitable for direct and *in situ* imaging of newly synthesized proteins (Ge et al., 2016; Starck et al., 2004). These methods require the irreversible reaction of the α-amino group of puromycin with the carbon on its carbonyl group, acylating the 3′ hydroxyl group of the peptidyl-tRNA buried in the P-site of the ribosome.

Motivated by the evidence that molecules containing puromycin modified at its α-amino group can bind the large subunit of the active ribosome (Schmeing et al., 2002), we covalently coupled puromycin to a biotin moiety through two 2,2′-ethylenedioxy-bis-ethylamine units to obtain a compound that is still able to bind ribosomes by mimicking the 3′-tRNA in the acceptor site (A-site). We synthesized the molecule (Figures 1A, 1B, and S1A), characterized it by nuclear magnetic resonance (NMR) and liquid chromatography-electrospray ionization-mass spectrometry (LC-ESI-MS) (Figures S1B and S1C), and called it 3P. We verified the activity of the biotin moiety, taking advantage of its absorbance spectrum, and tested the binding on polystyrene or

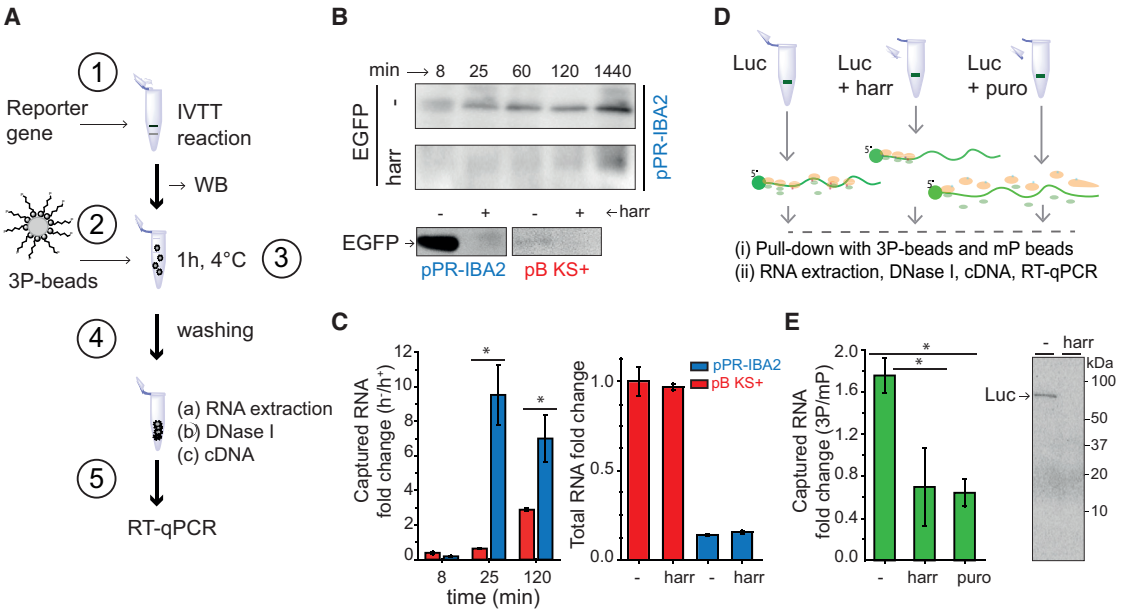

Figure 2. 3P-Functionalized Beads Can Capture mRNAs in Active Translation *In Vitro*

(A) Experimental design: 3P beads are used to pull down transcripts in a cell-free *in vitro* transcription-translation system. Briefly, from step 1 to step 5: (1) plasmids were added to the IVTT reaction mix, and the reaction was stopped by the addition of cycloheximide after 40 min; (2) beads were functionalized with 3P; (3) the IVTT reaction was incubated with 3P beads for 1 hr on a wheel at 2 rpm and 4°C; (4) beads were washed to remove unspecific binding; (4a) RNA was extracted and treated with DNase I to avoid possible DNA contaminations (4b); and (5) RNA samples were analyzed by RT-qPCR to detect the reporter gene.

(B) Immunoblotting of total EGFP protein at different incubation times, without (−) or with (+) harringtonine (2 μg/mL for 3 min). Immunoblotting showing the comparison between total EGFP expression from the pPR-IBA2 plasmid (blue) and EGFP expressed from the pBluescript II KS+ plasmid (red).

(C) EGFP RNA enrichment on RiboLace in the presence or absence of harringtonine (h−/h+) during time in different translational conditions: low (red pBluescript II KS+) and high translation efficiency (blue, pPR-IBA2 plasmid). At right, the total RNA content without (−) or with harringtonine (harr) in the two IVTT reactions; incubation time 25 min; t test; *$p < 0.05$.

(D) Experimental protocol for IVTT reaction with the firefly luciferase (luc) reporter with harringtonine (2 μg/mL for 3 min) or puromycin (puro, 40 min, 5 μg/mL) as controls of translation inhibition condition: (i) ribosomes in active translation were isolated with RiboLace, and mP beads were used as control for unspecific binding; (ii) RNA was extracted, treated with DNase I, and analyzed by qRT-PCR.

(E) Fold change values relative to the total amount of transcript captured by 3P beads were compared to the control beads (mP), henceforth referred to as the "enrichment." t test; *$p < 0.05$. All of the data presented represent the mean values and SDs of three to five independent experiments.

agarose beads. We observed that the biotin group allows the binding of 3P to commercially available streptavidin beads (Figure 1C).

To demonstrate that the 3P molecule maintains an inhibitory effect on translation, we compared its effects to that exerted by puromycin, using a eukaryotic *in vitro* cell-free transcription-translation system and the firefly luciferase as a reporter gene. We monitored total protein production by SDS-PAGE (Figure 1D) and luminescence assay (Figure S1D) in the presence of puromycin and 3P at different concentrations. As expected, puromycin induced conspicuous decay of protein production at nanomolar concentrations. In the case of 3P, we observed a decreased level of translation, which reached >70% of inhibition at concentrations >1 μM (Figure 1D). We concluded that even if it has slightly lower efficiency than puromycin, 3P can robustly inhibit eukaryotic translation *in vitro*, interfering with ribosome function, and can therefore be used to produce functionalized beads.

3P-Functionalized Beads Capture mRNAs in Active Translation *In Vitro*

Our finding that 3P is able to interact with the process of translation, likely through its puromycin moiety, prompted us to investigate whether 3P can capture mRNAs in active translation.

First, we monitored the ability of 3P-functionalized magnetic beads (3P beads) to purify transcripts of reporter genes with different levels of protein expression in *in vitro* translation systems. To this end, we developed the following protocol (Figure 2A): (1) *in vitro* transcription translation (IVTT) reaction to induce the production of the reporter protein, (2) functionalization of beads with 3P, (3) stopping reaction with the translation inhibitor cycloheximide and incubation of 3P beads and control beads functionalized with a biotin-glycol conjugate (mP beads), (4) washing of beads, and (5) extraction of RNA associated with the beads for downstream analyses. In parallel, the production of the protein was followed by detection of whole protein extracts.

We applied this protocol to study the ability of our 3P functionalized beads to purify mRNAs associated with high translational states. We took advantage of two reporter plasmids characterized by different translational efficiencies. The EGFP reporter genes showed differential efficiency in protein production, depending on the expression vector used (IPR-IBA2) (Arosio

et al., 2007), high performance and pBluescript II KS+ (Higashi et al., 2006), and low performance (Figure 2B). Complete inhibition of protein production was observed after addition of the translation inhibitor harringtonine as a control (Figure 2B). We applied our protocol, purified the RNA associated with the beads, and quantified by RT-qPCR the relative abundance of EGFP mRNA in both low- and high-performance conditions (Figure 2C). We observed a 7- to 10-fold enrichment of the reporter transcript on 3P functionalized beads in conditions of active translation, with respect to samples treated with harringtonine. This enrichment can be observed in the absence of transcriptional changes (Figure 2C, right) and with respect to the unspecific binding on control beads (Figure S2).

Then, to demonstrate that this result was not dependent on the reporter used, we applied the methodology to a luciferase reporter system (Figures 2D and 2E). In this case, we observed a >1.6-fold enrichment of luciferase transcript with respect to negative controls (mP beads) and an enrichment with respect to samples in which translation had been inhibited (Figure 2D), as previously observed for EGFP. Finally, to understand whether the observed enrichments were dependent on the puromycin moiety of 3P, we pre-saturated the system with puromycin and induced ribosome drop-off. Under these conditions, we found no evidence for mRNA enrichment (Figure 2E). Overall, these findings support the claim that 3P beads can be used to capture transcripts undergoing translation in eukaryotic *in vitro* systems. We named this method RiboLace.

RiboLace Captures Active Ribosomes and Associated mRNAs from Whole Cellular Lysates

Next, we wanted to establish whether RiboLace was capable of isolating ribosomes and mRNAs under active translation from more complex systems than *in vitro* mixtures. We used RiboLace on whole cellular lysates under different translational states and monitored its efficiency to capture mRNAs and proteins associated with ribosomes and polysomes in cellular lysates (Figure 3A). We took advantage of established cellular stimuli that induce cells into translationally active or inactive states. To shut down translation, we used cell starvation and oxidative, proteotoxic, and heat stresses, all of which are known to globally suppress protein synthesis (Liu and Qian, 2016) (Figure S3A). To specifically activate protein synthesis, we rescued cells from starvation by epithelial growth factor (EGF) or by fetal bovine serum (FBS) stimulation (Thomas et al., 1982).

First, we monitored the enrichment on RiboLace of functional and structural markers of ribosomes (eukaryotic elongation factor 1α [eEF1α], calnexin, RPL26, and RPS6) in lysates of immortalized human cells (HEK293T) (Figure 3B). We used 2×10^5 cells, representing ~1/40 of the input material required for classical polysomal profiling or ribosome profiling approaches. The elongation factor eEF1α is responsible for the delivery of aminoacyl-tRNAs to the translation machinery and is associated with ribosomes in active translation (Andersen et al., 2001; Lamberti et al., 2004). Calnexin is a chaperone protein in the endoplasmic reticulum that associates with ribosomes, helping protein folding during translation (Lakkaraju et al., 2012). Finally, RPL26 and RPS6 are ribosomal proteins belonging to the large and small subunits of the ribosome, respectively. After immunoblotting the RiboLace-eluted proteins from untreated cells, we observed an enrichment of all four proteins with respect to serum starvation. When cells were stimulated with EGF after starvation, we observed a modest increase in the signal of the translational markers (Figures 3B and 3C). Because the background signal using control beads (mP beads) was the same in all conditions, our results suggest that RiboLace can pull down active ribosomes, therefore monitoring the translational state of cells.

To further confirm this result, we monitored the relative abundances on RiboLace of eEF1α and eEF2 between no-stress and stress conditions. It is known that eEF2-mediated translocation and the switch of ribosome conformation from the non-rotated to the rotated state (Lareau et al., 2014) are inhibited by cycloheximide (Schneider-Poetsch et al., 2010). In agreement with the hypothesis that RiboLace captures active ribosomes, we found that RiboLace can isolate both proteins, with preferential enrichment of eEF1α with respect to eEF2 (Figure 3D), reflecting the co-sedimentation profile of the two proteins with polysomes (Figure S3B). This finding suggests that RiboLace favors the capture of the non-rotated conformation of the ribosome (Ferguson et al., 2015). Because the duration of cycloheximide treatment is a few minutes long and the elongation speed of translation is ~6 amino acids (aa)/s (Ingolia et al., 2011), RiboLace is likely able to capture ribosomes that are in a different phase of the elongation cycle at the beginning of the treatment (i.e., after peptide bond formation but before translocation). In fact, the cycloheximide treatment is long enough for ribosomes in the pre-translocation stage to move into the post-translocation cycle, be blocked by the drug, and be captured by RiboLace.

Next, we tested RiboLace in a different cell line, the widely used human tumor cell line MCF7, under control or starvation conditions, establishing again the presence of translational markers associated with RiboLace (Figure 3E). In addition to ribosomal proteins, we detected other proteins known to be associated with polysomes (e.g., PABP, eIF4B) or to be a marker of active translation (me(K9)H3) (Rivera et al., 2015), while proteins not associated with polysomes did not show any enrichment (Figure S3C). In agreement with results obtained for HEK293T cells, the decrease in translational markers associated with RiboLace in starved cells suggests that our method captures fewer ribosomes when global translation is downregulated. To further validate this finding, we applied other stress stimuli known to elicit repression of global protein synthesis (e.g., proteotoxic stress, heat shock, sodium arsenite). In all of the cases, translation markers were reduced (Figure S3D). We then tested RiboLace on a mouse motor neuron-like cell line, NSC-34, under normal growth conditions. We observed an ~8-fold enrichment of RPL26 and an ~4-fold enrichment of RPS6 with respect to control beads (Figure S3E), demonstrating that RiboLace can isolate ribosomes from both human and mouse cell lines.

Consistent with these results, the pelota protein (mammalian ortholog of the yeast Dom34), known to promote the dissociation of stalled ribosomes (Guydosh and Green, 2014; Pisareva et al., 2011), was not enriched in RiboLace applied to control, starved, or arsenite-treated lysates of MCF7 and HEK293T cells (Figures 3F and S3F, respectively).

These findings prompted us to investigate whether RiboLace provides an improved estimation of protein level with respect

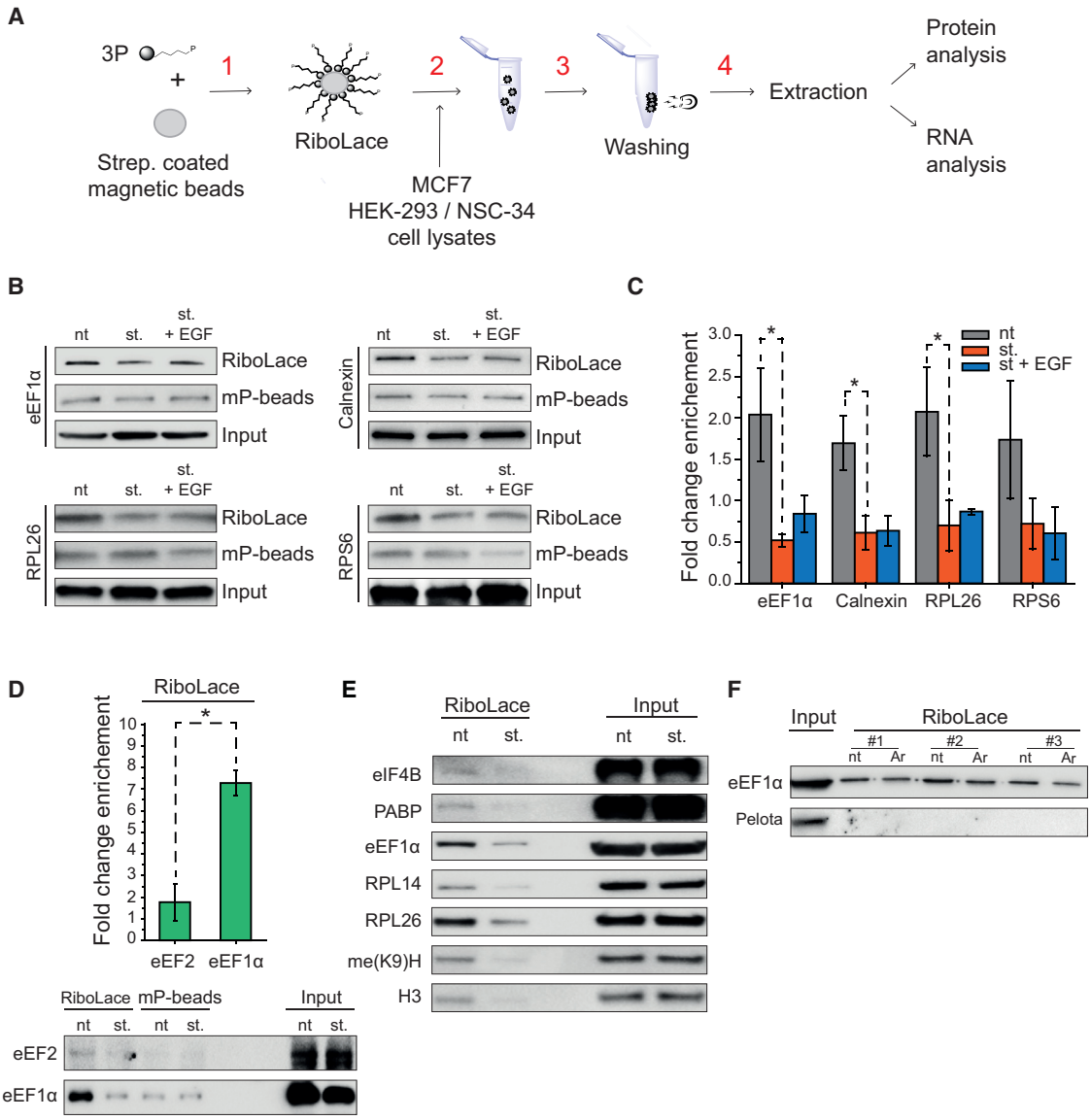

Figure 3. RiboLace Is Able to Capture Ribosomes and Associated mRNAs under Active Translation in Cell Cultures and Tissues

(A) RiboLace protocol: magnetic beads coated with streptavidin are functionalized with the 3P molecule (step 1). RiboLace beads are then added to the cell lysate (step 2) (usually 5–20 μL, corresponding to ~1.2–5 × 10^5 cells) and washed (step 3). Finally, both proteins and RNA are recovered for further analysis (step 4).

(B) Immunoblotting of eEF1α, calnexin, RPL26, and RPS6 isolated after applying the RiboLace protocol on HEK293 cells (RiboLace, mP beads, and input).

(C) Quantification of proteins isolated with RiboLace under different stress conditions. n = 3; t test; *p < 0.05.

(D) Comparison between the relative enrichment (no starvation versus starvation) of eEF2 and eEF1α on RiboLace. t test; *p < 0.05; n = 4.

(E) Immunoblotting of eIf4B, PABP, eEF1α, RPL14, RPL26, me(K9)H3, and H3, detected on RiboLace under normal growing conditions (nt) or serum starvation (st), with relative inputs in MCF7 cytoplasmic lysates.

(F) Immunoblotting of pelota and eEF1α detected on RiboLace in MCF7 treated or not treated with arsenite.

to the use of total RNA or polysomal RNA (Figure 4A). To this end, we compared at transcriptome-wide scale the proteome of MCF7 cells with all three RNA quantifications: total RNA levels (classical transcriptome), polysomal RNA levels (classical translatome), and RiboLace. The levels of ~2,700 proteins were determined by MS and label-free quantification (LFQ). We report in Figure 4B (left) that RNA levels obtained using RiboLace displayed the highest correlation with protein levels (0.48), significantly improving the correlation obtained with polysomal RNA (0.41) and total RNA (0.18). It is worth mentioning that some translational changes may show up as a shift in the position of an mRNA within a sucrose density gradient rather than as a change in the fraction of the mRNA found in polysomes, thereby penalizing the sensitivity of polysome-associated RNA sequencing. Our results prove that RiboLace provides a reliable estimation of the translation state of cells.

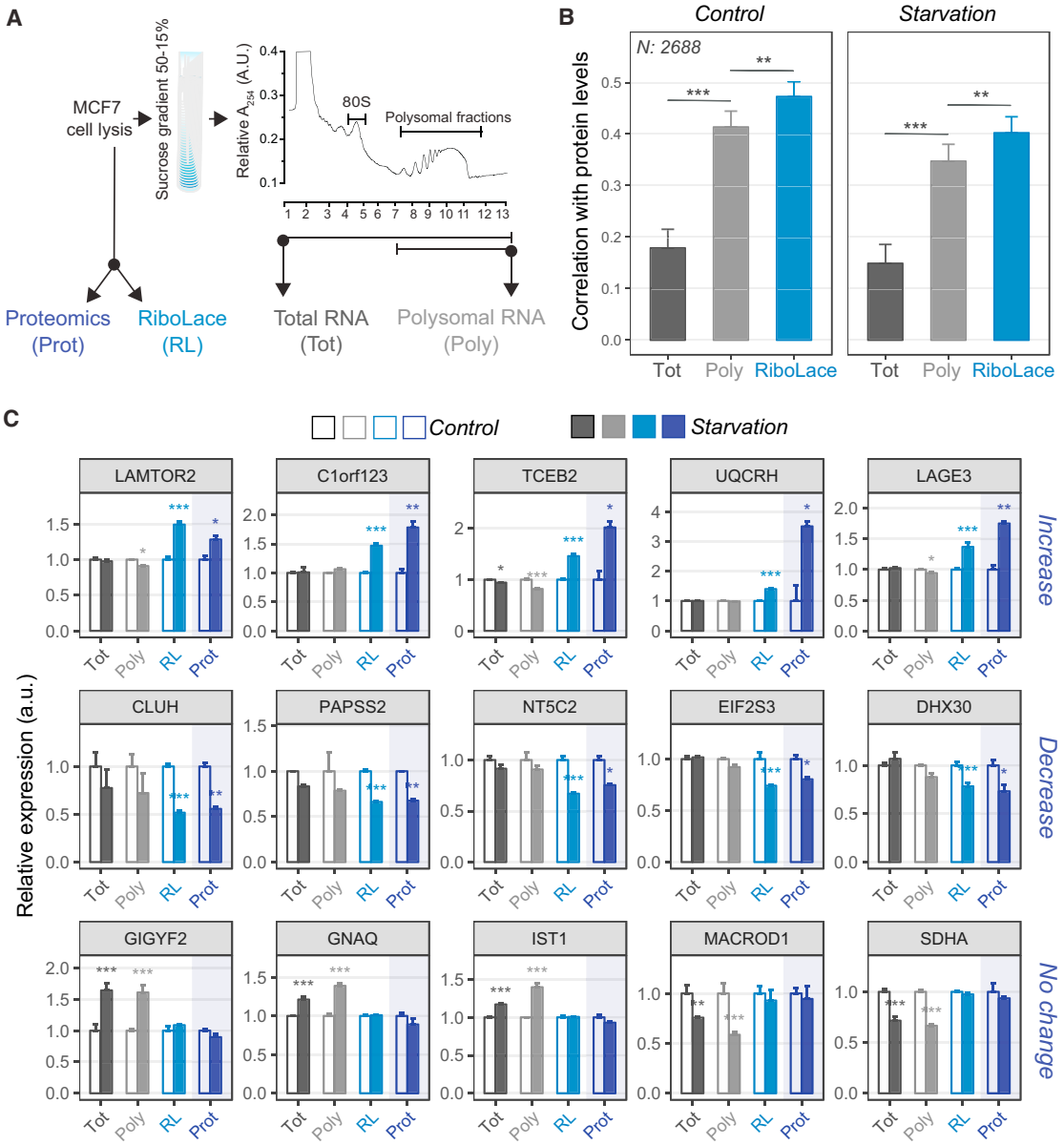

Figure 4. Comparison of RiboLace to RNA-Seq or POL-Seq Reveals that RiboLace Is an Accurate Proxy of the Cellular Proteome

(A) Experimental design for comparing the global RNA repertoire of RNAs associated with RiboLace by next-generation sequencing, total RNA sequencing (RNA-seq), and polysomal sequencing (POL-seq) to the cellular proteome.

(B) Correlation analysis between the MCF7 proteome, determined by mass spectrometry, and total RNA, polysomal RNA, and RiboLace RNA, respectively, determined by deep sequencing. Pearson correlation values are displayed (error bars refer to the 95% confidence interval). The significance of the differences between Pearson coefficients was measured using Williams' test (**$p < 0.01$, ***$p < 0.001$).

(C) Single gene comparisons of protein (Prot), RiboLace (RL), polysomal RNA (Poly), and total RNA (Tot) levels in MCF7 control and starved cells (empty and filled bars, respectively). Data are represented as means ± SEMs (*$p < 0.05$, **$p < 0.01$, and ***$p < 0.001$, based on proteomics or next-generation sequencing [NGS] differential analysis). A total of 15 representative genes, with the most significant differences between RiboLace and conventional approaches, were chosen for display, showing either increase (top row), decrease (middle row), or no change (bottom row) at the protein level.

To further validate these results, we isolated RNA from total RNA, polysomal RNA, and RiboLace from MCF7 cells before and after serum starvation or EGF stimulation (Figures S4A–S4F). As in control cells (Figure 4B, left), we observed in starved MCF7 cells a significantly higher correlation between protein levels and RiboLace levels with respect to polysomal and total RNA levels (Figure 4B, right). We next searched for genes that contributed the most to this difference in correlation. Comparing the control and starved conditions, we considered cases in which significant protein changes were reported in

proteomics. We identified a population of 80 genes changing at the protein and mRNA levels in proteomics and RiboLace, respectively. The mRNA shifts of these 80 genes were either not detected or reversed at both polysomal and total RNA levels (Figure 4C, upper row for upregulated proteins and middle row for downregulated proteins).

Next, we considered a scenario in which the researcher would exclude unchanging proteins from the analysis of translation. We found a population of 201 genes showing no change in protein levels and no change in RiboLace levels, but showing significant changes in polysomal and optionally total RNA levels (Figure 4C, bottom row). For each of these populations, five representative genes showing the most significant differences between RiboLace and conventional approaches were chosen for display (Figure 4C). Further validations for the consistency between RiboLace measurements and protein levels in the case of MCF7 cells treated with EGF are provided in Figures S4D–S4F.

Overall, these results establish the important proof-of-concept that RiboLace can capture ribosomes under active translation and estimate protein levels and their variations with accuracy and reliability.

In Vivo Active Ribosome Profiling Using RiboLace: Active Ribo-Seq

Given the unique opportunity to purify active ribosomes from low amounts of input material, we next wanted to combine our purification strategy with Ribo-seq to capture active ribosome dynamics along transcripts, thereby improving ribosome profiling experiments. To facilitate this, we modified our original protocol by including an endonuclease digestion step and applying it to cellular and tissue lysates (Figure 5A).

First, we demonstrated that RiboLace can capture isolated ribosomes after endonuclease digestion, as shown by the enrichment of eEF1α, calnexin, RPL26, and RPS6 on RiboLace in HEK293T and HeLa cells (Figure 5B). Second, we confirmed that RiboLace was able to enrich ribosome-protected fragments (Figures S5A and S5B). Third, we applied RiboLace on as few as 15 μL of whole mouse brain ribosome-protected fragments (RPFs). In parallel, we performed ribosome profiling from polysomes, pre-purified using sucrose gradients (750 μL of total brain lysate, Ribo-seq; Figure 5C). After sequencing, we analyzed both RiboLace and Ribo-seq ribosome-protected fragments using the dedicated pipeline riboWaltz (Lauria et al., 2018) to obtain sub-codon information and identification of the trinucleotide periodicity. The distribution of read lengths highlighted a main population of ribosome-protected fragments at ~29 nt (Figure S5C) (Archer et al., 2016; Lareau et al., 2014). As expected for ribosome footprints, we observed an enrichment of signal from mapped reads along coding sequence regions in both RiboLace and Ribo-seq data (Figure 5D), demonstrating that RiboLace is indeed able to capture bona fide ribosomes. Occupancy meta-profiles, derived from the aggregation of signals on single genes, presented the typical trinucleotide periodicity of the ribosome P-site along coding sequences, which is suggestive of signal derived from ribosomes moving along transcripts (Figures 5E and 5F). The comparison between meta-profiles obtained with RiboLace and Ribo-seq highlights for our method an accumulation of ribosomes at the start codon and at the fifth codon, a feature that has previously been reported to be associated with a productive elongation phase of translation (Han et al., 2014).

To further reinforce our findings, we systematically compared position-specific profiles from RiboLace and standard Ribo-seq using an additional dataset from the widely used HEK293 human cell line (Figure S6A). According to Arava et al. (2003), in fully growing, actively translating cells, an overall decrease of ribosome density is expected along the transcripts. We therefore analyzed our data by calculating the ratio between the average number of P-sites on the coding sequence and the average number of P-sites on the first five codons for each transcript. The lower this value, the lower the ribosome density ratio along the transcript. By comparing the distributions obtained with RiboLace and Ribo-seq, RiboLace showed a stronger decrease in ribosome density along coding sequences than Ribo-seq, both in mouse brain and in HEK293 cells (Figure 6A), which is in line with active translation (Arava et al., 2003). Conversely, a comparison of codon-specific ribosome densities revealed a high correlation between RiboLace and Ribo-seq (0.98 in mouse brains and 0.93 in HEK293 cells), suggesting the absence of differences at this general level.

Finally, we compared gene-specific translation estimates obtained using RiboLace and Ribo-seq. In this way, we identified populations of genes whose translation signal was specifically enriched in either RiboLace or Ribo-seq (Figure 6B). This result shows that, for both case studies we generated, the two techniques significantly differ in translation estimates for hundreds of genes. Functional enrichment analysis of these populations suggested that RiboLace-enriched transcripts were more pertinent to the biological system under study (embryonic kidney cells and brain extracts, respectively) in comparison to Ribo-seq-enriched transcripts (Figure 6C). In addition, RiboLace-specific transcripts were enriched for translation-related genes in both datasets (Figure 6C).

These results demonstrate that RiboLace is capable of providing positional data of active ribosomes with nucleotide resolution, starting from much less material than available protocols, thereby facilitating reliable descriptions of bona fide translational events *in vitro* and *in vivo*.

DISCUSSION

During their lifetime in the cytoplasm, mRNAs are regularly stored, degraded, and transported, with only a fraction being actively translated to produce proteins at a specific point in time (Morisaki et al., 2016; Wu et al., 2016). We estimated this fraction to be between 80% and 60% of the total population, depending on the cell type (Figure S6). All of these stages of the mRNA life cycle are governed by *cis*- and *trans*-factors that tightly regulate the uploading of mRNAs on polysomes and the subsequent production of proteins. To generate an improved understanding of these sophisticated and dynamic processes, different methodological approaches have been developed to determine, at the genome-wide scale, changes in RNA steady-state levels (e.g., RNA sequencing [RNA-seq]), their engagement with the translational machinery (e.g., Ribo-seq, polysomal profiling) (Ingolia et al., 2011; Tebaldi et al., 2012), and changes in protein production (e.g., stable isotope labeling by amino

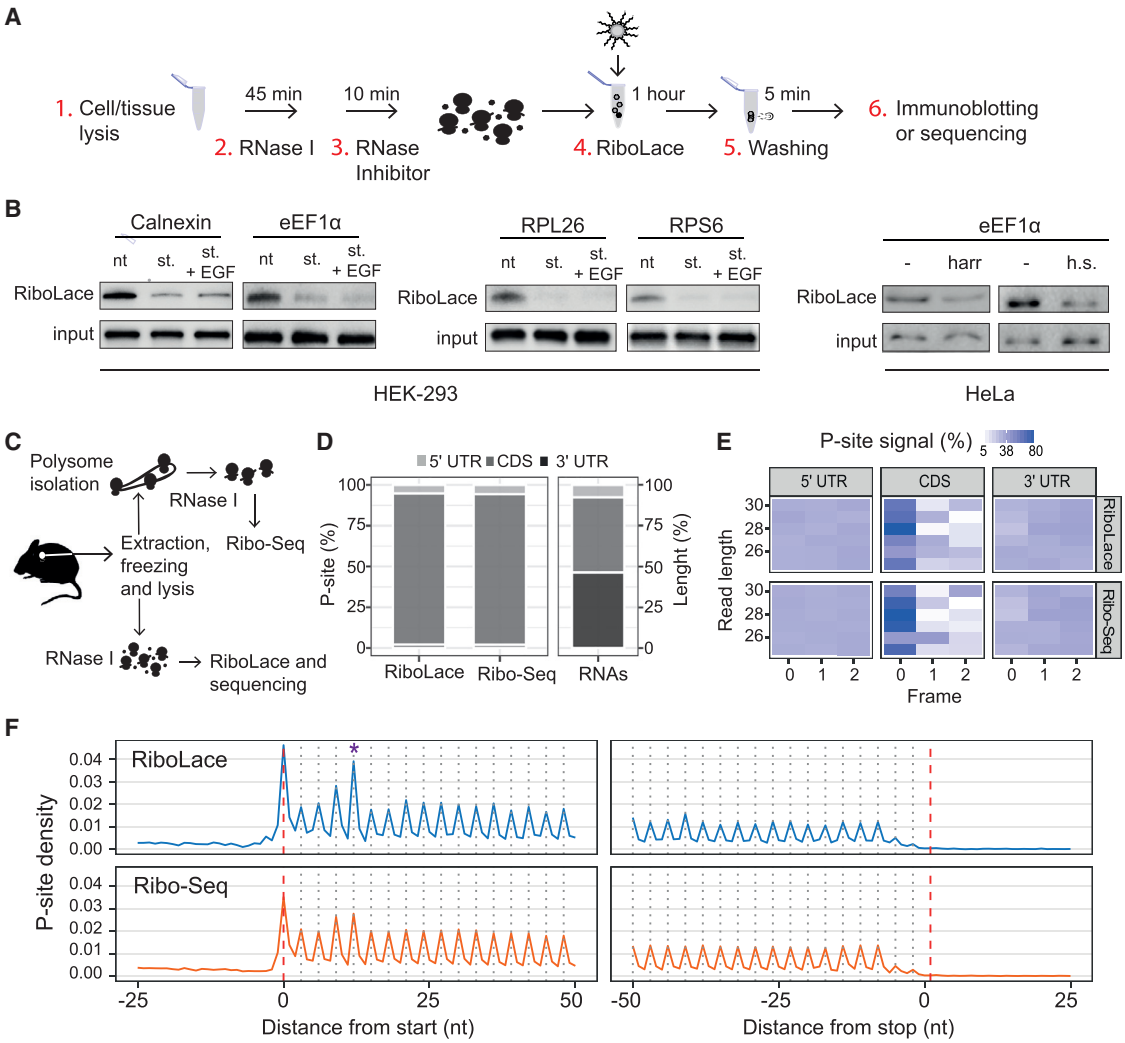

Figure 5. Active Ribosome Profiling with RiboLace

(A) Schematic overview of the RiboLace protocol for the separation of ribosome-protected fragments from active ribosomes. (1) Cell lysates are prepared and (2) treated with RNase I for 45 min; (3) the endonuclease digestion is stopped with an RNase inhibitor; (4) RiboLace beads are incubated with the digested cell lysate and (5) washed to remove specifically bound molecules, (6) proteins, or RNA extracted.

(B) Immunoblotting of eEF1α, calnexin, RPL26, and RPS6 after applying the protocol described in (A) in HEK293 and HeLa. harr, harringtonine treatment; h.s., heat shock; nt., not treated; st., starvation (0.5% FBS); st. + EGF, starvation followed by the addition of EGF.

(C) Schematic overview of the protocol for parallel RiboLace Ribo-seq in mouse brain.

(D) Left, percentage of P-sites mapping to the 5′ UTR, coding sequence (CDS), and 3′ UTR of mRNAs from RiboLace and Ribo-seq data. Right, length percentage of each mRNA region.

(E) Percentage of P-sites corresponding to the three possible reading frames in RiboLace (top) and Ribo-seq (bottom) along the 5′ UTR, CDS, and 3′ UTR, stratified for read length. For each length and each region, the sum of the signal is normalized to 100%.

(F) Meta-gene profiles showing the density of P-sites around translation initiation sites (TISs) and translation termination sites (TTSs) for RiboLace (top) and Ribo-seq (bottom). The peak corresponding to the fifth codon is highlighted with an asterisk.

acids in cell culture [SILAC], puromycin-associated nascent chain proteomics [PUNCH-P]) (Aviner et al., 2014; Liu et al., 2017; Ong and Mann, 2006). Although Ribo-seq remains a complex technology that requires relatively large volumes of experimental material, it has been shown to be extremely powerful for identifying ORFs and translation initiation sites from (1) cell lysates or ribosome pellets; (2) purified polysomal fractions (Juntawong et al., 2014); or, more recently, (3) tagged ribosomes (Jan et al., 2014; Shi et al., 2017). Unfortunately, however, the use of cell lysates and ribosome pellets often introduces unwanted background signals.

Here, we specifically designed RiboLace for ribosome profiling experiments, to facilitate understanding of ribosome dynamics along transcripts and to allow accurate estimates of translation levels based on active ribosome footprints. We sought to enhance Ribo-seq approaches by developing a

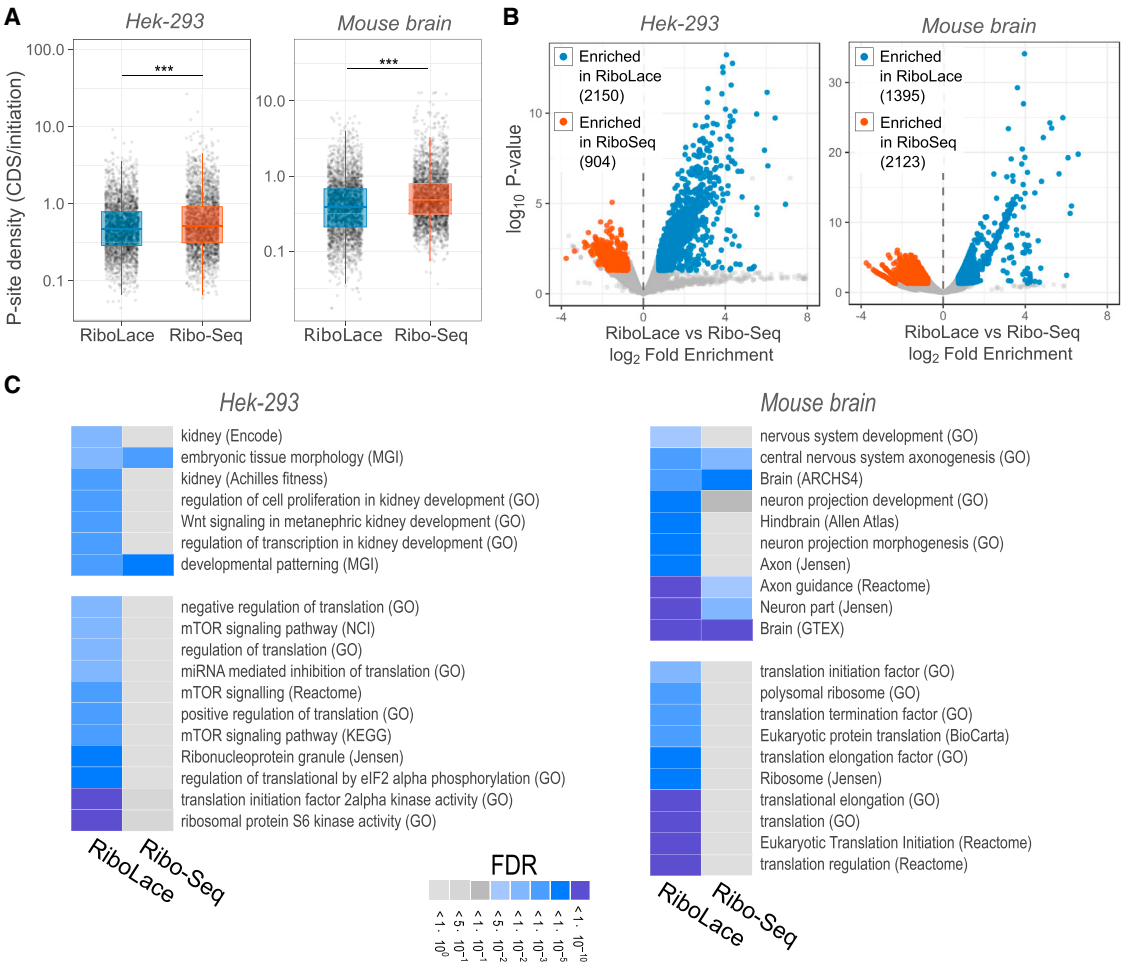

Figure 6. RiboLace versus Ribo-Seq

(A) Dot plots showing the distribution of the ratios between the average number of P-sites on the CDS and the average number of P-sites on the first five codons for RiboLace and Ribo-seq performed in HEK293 (left) and in mouse brain (right). The boxplots associated with the distributions are also reported, along with the statistical significances from the Wilcoxon-Mann-Whitney test (***$p < 0.001$).

(B) Volcano plots comparing RiboLace and Ribo-seq transcript-specific translation estimates in HEK293 cells (left) and mouse brains (right). For each transcript, the log2 fold enrichment of translation estimates (RiboLace versus Ribo-seq) was plotted against the statistical significance of the fold enrichment. Significantly enriched transcripts are highlighted.

(C) Comparative annotation enrichment analysis of transcripts enriched in RiboLace and Ribo-seq in HEK293 cells (left) and mouse brains (right). The heatmap is colored according to the significance of the enrichments. The analysis was performed on terms related to the specific biological system under consideration (upper block) and to translation (lower block).

molecule (3P) that facilitates the selective capture of ribosomes under active translation. We focused our attention on puromycin, the well-known structural analog of the 3′ end of aminoacyl-tRNA, and tethered the α-amino group to a biotinylated linker. We observed that 3P can interfere with eukaryotic translation *in vitro*. We used 3P- functionalized beads (RiboLace) to capture and enrich transcripts undergoing translation in eukaryotic *in vitro* and *in vivo* systems. We observed that the elongation factor eEF1α, a key protein involved in delivering tRNAs to the ribosome, was the most enriched protein on RiboLace in all of our experiments. This suggests that in the presence of cycloheximide treatments, 3P binding to the A-site of the ribosome in the not-rotated state of the ribosome (Ferguson et al., 2015; Lareau et al., 2014) is favored. Given the elongation speed of ~6 aa/s (Ingolia et al., 2011) and the duration of cycloheximide treatment, all ribosomes in a different phase of the elongation cycle at the beginning of the treatment (i.e., after peptide bond formation but before translocation) have more than enough time to move into the post-translocation cycle, be blocked by cycloheximide, and be captured by RiboLace.

Comparing RiboLace sequencing with proteomics on a transcriptome-wide scale, we obtained evidence to suggest that RiboLace is a powerful and reliable alternative to quantify the translation state of cells compared to standard transcriptome and translatome profiling methods. We then demonstrated that RiboLace is capable of providing positional data with nucleotide resolution of translational events when used for ribosome profiling, requiring ~40 times less material than current

Ribo-seq protocols. We observed that >95% of ribosome-protected fragments were mapped on the coding region, with the characteristic trinucleotide periodicity suggestive of active ribosomes flowing along the transcripts and almost no signal on either the 5′- and 3′-UTRs of mRNAs.

We showed in two different case studies that RiboLace and Ribo-seq significantly differ in translation estimates for hundreds of genes. Functional annotation analysis suggests that RiboLace-enriched transcripts are more pertinent to the biological system under study with respect to Ribo-seq-enriched transcripts. In addition, RiboLace-specific transcripts are enriched for translation-related genes.

Overall, our data suggest that RiboLace is an effective approach for ribosome profiling experiments, in terms of required-sample input and accuracy in ribosome-protected fragments detection. RiboLace protocols can be further adjusted to (1) isolate ribosomes from other organisms than human and mouse or to (2) isolate ribosomes from specific eukaryotic cellular compartments such as the endoplasmic reticulum or organelles such as mitochondria.

In summary, RiboLace can be used to capture ribosomes in active translation with challenging or troublesome biological samples with low-input material for reliable ribosome profiling. Our method empowers scientists to efficiently and reproducibly determine the actual translational state of a biological system.

STAR★METHODS

Detailed methods are provided in the online version of this paper and include the following:

- KEY RESOURCES TABLE
- CONTACT FOR REAGENT AND RESOURCE SHARING
- EXPERIMENTAL MODEL AND SUBJECT DETAILS
  - Tissues, cell lines and growth conditions
- METHOD DETAILS
  - Chemical synthesis of the 3P molecule
  - Depletion assay of 3P with streptavidin coated beads
  - *In vitro* - cell free Transcription/Translation
  - Preparation of RiboLace beads
  - RiboLace and IVTT system
  - Luciferase assay
  - Purification of active polysomes and ribosomes with RiboLace
  - RNA extraction for RNA-Seq and POL-Seq
  - Immunoblotting
  - qPCR
  - Protein sample preparation for MS
- QUANTIFICATION AND STATISTICAL ANALYSIS
  - Data analysis of RNA-seq and POL-seq experiments
  - Data analysis of MS
  - Data analysis of ribosome profiling experiments
- DATA AND SOFTWARE AVAILABILITY

SUPPLEMENTAL INFORMATION

Supplemental Information includes six figures and three tables and can be found with this article online at https://doi.org/10.1016/j.celrep.2018.09.084.

ACKNOWLEDGMENTS

We thank Tocris Bioscience (a Biotechne brand) for the support in scaling up the 3P synthesis. We thank Veronica De Sanctis and Roberto Bertorelli of the Centre for Integrative Biology Next Generation Sequencing (CIBIO NGS) core facility; Myriam Demant and Marc Guender of Thermo Fisher Scientific, Switzerland, for acquiring the proteomics data; and Romina Belli from the CIBIO MS core facility for technical support. We thank Daniele Arosio for the kind gift of the IPR-IBA2 plasmid. This work was supported by IMMAGINA BioTechnology s.r.l. and the Provincia Autonoma di Trento, Italy (AxonomiX research project), with additional grant funding from the Wellcome Trust (106098/Z/14/Z to E.J.N.G. and T.H.G.) and the SMA Trust (UK SMA Research Consortium) (to T.H.G.).

AUTHOR CONTRIBUTIONS

M.C. and G.V. conceived the experiments. M.C. performed all the biological experiments and contributed to the 3P synthesis. T.T. analyzed the proteomics and next-generation sequencing data. T.T., D.G., and F.L. analyzed the RNA-seq and Ribo-seq data. P.B., M.C., and E.P. performed the Ribo-seq and RiboLace. M.M. and G.V. performed the ribosome drop-off experiments. M.M. prepared the samples for the proteomics analysis. D.T.K. and L.P. performed the control experiments. L.M. helped with the Ribo-seq set-up experiments. R.F.G.B. performed a preliminary synthesis of 3P. G.G. designed the 3P synthesis and performed the MS, correlation spectroscopy (COSY), and NMR analyses of the 3P. E.J.N.G. and T.H.G. generated and provided the mouse tissues. M.C. and G.V. drafted the manuscript. G.V., M.C., T.T., F.L., G.G., E.J.N.G., T.H.G., and A.Q. reviewed the manuscript. All of the authors read and approved the final manuscript.

DECLARATION OF INTERESTS

M.C. is the founder of, director of, and a shareholder in IMMAGINA BioTechnology s.r.l., a company engaged in the development of new technologies for gene expression analysis at the ribosomal level. A.Q. is on the board of directors of IMMAGINA BioTechnology s.r.l. A.Q. and G.G. are shareholders in IMMAGINA BioTechnology s.r.l. G.V. is the scientific advisor of IMMAGINA BioTechnology s.r.l. All of the other authors declare no competing interests. RiboLace is an IMMAGINA BioTechnology s.r.l.-patented technology (WO2017013547 A1 - PCT/IB2016/054210).

Received: November 6, 2017
Revised: April 20, 2018
Accepted: September 25, 2018
Published: October 23, 2018

REFERENCES

Aeschimann, F., Xiong, J., Arnold, A., Dieterich, C., and Grosshans, H. (2015). Transcriptome-wide measurement of ribosomal occupancy by ribosome profiling. Methods *85*, 75–89.

Andersen, G.R., Valente, L., Pedersen, L., Kinzy, T.G., and Nyborg, J. (2001). Crystal structures of nucleotide exchange intermediates in the eEF1A-eEF1Balpha complex. Nat. Struct. Biol. *8*, 531–534.

Arava, Y., Wang, Y., Storey, J.D., Liu, C.L., Brown, P.O., and Herschlag, D. (2003). Genome-wide analysis of mRNA translation profiles in Saccharomyces cerevisiae. Proc. Natl. Acad. Sci. USA *100*, 3889–3894.

Archer, S.K., Shirokikh, N.E., Beilharz, T.H., and Preiss, T. (2016). Dynamics of ribosome scanning and recycling revealed by translation complex profiling. Nature *535*, 570–574.

Arosio, D., Garau, G., Ricci, F., Marchetti, L., Bizzarri, R., Nifosì, R., and Beltram, F. (2007). Spectroscopic and structural study of proton and halide ion cooperative binding to gfp. Biophys. J. *93*, 232–244.

Aviner, R., Geiger, T., and Elroy-Stein, O. (2014). Genome-wide identification and quantification of protein synthesis in cultured cells and whole tissues by

puromycin-associated nascent chain proteomics (PUNCH-P). Nat. Protoc. *9*, 751–760.

Bazzini, A.A., Johnstone, T.G., Christiano, R., Mackowiak, S.D., Obermayer, B., Fleming, E.S., Vejnar, C.E., Lee, M.T., Rajewsky, N., Walther, T.C., and Giraldez, A.J. (2014). Identification of small ORFs in vertebrates using ribosome footprinting and evolutionary conservation. EMBO J. *33*, 981–993.

Bernabò, P., Tebaldi, T., Groen, E.J.N., Lane, F.M., Perenthaler, E., Mattedi, F., Newbery, H.J., Zhou, H., Zuccotti, P., Potrich, V., et al. (2017). In vivo translatome profiling in spinal muscular atrophy reveals a role for SMN protein in ribosome biology. Cell Rep. *21*, 953–965.

Bhat, M., Robichaud, N., Hulea, L., Sonenberg, N., Pelletier, J., and Topisirovic, I. (2015). Targeting the translation machinery in cancer. Nat. Rev. Drug Discov. *14*, 261–278.

Biyani, M., Husimi, Y., and Nemoto, N. (2006). Solid-phase translation and RNA-protein fusion: a novel approach for folding quality control and direct immobilization of proteins using anchored mRNA. Nucleic Acids Res. *34*, e140.

Chapman, R.E., and Walter, P. (1997). Translational attenuation mediated by an mRNA intron. Curr. Biol. *7*, 850–859.

Chew, G.-L., Pauli, A., Rinn, J.L., Regev, A., Schier, A.F., and Valen, E. (2013). Ribosome profiling reveals resemblance between long non-coding RNAs and 5′ leaders of coding RNAs. Development *140*, 2828–2834.

Darnell, J.C., Van Driesche, S.J., Zhang, C., Hung, K.Y.S., Mele, A., Fraser, C.E., Stone, E.F., Chen, C., Fak, J.J., Chi, S.W., et al. (2011). FMRP stalls ribosomal translocation on mRNAs linked to synaptic function and autism. Cell *146*, 247–261.

David, A., Dolan, B.P., Hickman, H.D., Knowlton, J.J., Clavarino, G., Pierre, P., Bennink, J.R., and Yewdell, J.W. (2012). Nuclear translation visualized by ribosome-bound nascent chain puromycylation. J. Cell Biol. *197*, 45–57.

Doma, M.K., and Parker, R. (2006). Endonucleolytic cleavage of eukaryotic mRNAs with stalls in translation elongation. Nature *440*, 561–564.

Ferguson, A., Wang, L., Altman, R.B., Parks, M.M., Vincent, C.T., Blanchard, S.C., Ferguson, A., Wang, L., Altman, R.B., Terry, D.S., et al. (2015). Functional dynamics within the human ribosome regulate the rate of active protein synthesis. Mol. Cell *60*, 475–486.

Fioriti, L., Myers, C., Huang, Y.-Y., Li, X., Stephan, J.S., Trifilieff, P., Colnaghi, L., Kosmidis, S., Drisaldi, B., Pavlopoulos, E., and Kandel, E.R. (2015). The persistence of hippocampal-based memory requires protein synthesis mediated by the prion-like protein CPEB3. Neuron *86*, 1433–1448.

Fritsch, C., Herrmann, A., Nothnagel, M., Szafranski, K., Huse, K., Schumann, F., Schreiber, S., Platzer, M., Krawczak, M., Hampe, J., and Brosch, M. (2012). Genome-wide search for novel human uORFs and N-terminal protein extensions using ribosomal footprinting. Genome Res. *22*, 2208–2218.

Gambetti, P., Hirt, L., Stieber, A., and Shafer, B. (1972). Distribution of puromycin peptides in mouse entorhinal cortex. Exp. Neurol. *34*, 223–228.

Ge, J., Zhang, C.-W., Ng, X.W., Peng, B., Pan, S., Du, S., Wang, D., Li, L., Lim, K.-L., Wohland, T., and Yao, S.Q. (2016). Puromycin analogues capable of multiplexed imaging and profiling of protein synthesis and dynamics in live cells and neurons. Angew. Chem. Int. Ed. Engl. *55*, 4933–4937.

Goyer, C., Altmann, M., Lee, H.S., Blanc, A., Deshmukh, M., Woolford, J.L., Jr., Trachsel, H., and Sonenberg, N. (1993). TIF4631 and TIF4632: two yeast genes encoding the high-molecular-weight subunits of the cap-binding protein complex (eukaryotic initiation factor 4F) contain an RNA recognition motif-like sequence and carry out an essential function. Mol. Cell. Biol. *13*, 4860–4874.

Graber, T.E., Hébert-Seropian, S., Khoutorsky, A., David, A., Yewdell, J.W., Lacaille, J.-C., and Sossin, W.S. (2013). Reactivation of stalled polyribosomes in synaptic plasticity. Proc. Natl. Acad. Sci. USA *110*, 16205–16210.

Guydosh, N.R., and Green, R. (2014). Dom34 rescues ribosomes in 3′ untranslated regions. Cell *156*, 950–962.

Han, Y., Gao, X., Liu, B., Wan, J., Zhang, X., and Qian, S.-B. (2014). Ribosome profiling reveals sequence-independent post-initiation pausing as a signature of translation. Cell Res. *24*, 842–851.

Higashi, K., Kashiwagi, K., Taniguchi, S., Terui, Y., Yamamoto, K., Ishihama, A., and Igarashi, K. (2006). Enhancement of +1 frameshift by polyamines during translation of polypeptide release factor 2 in Escherichia coli. J. Biol. Chem. *281*, 9527–9537.

Higashi, S., Kabuta, T., Nagai, Y., Tsuchiya, Y., Akiyama, H., and Wada, K. (2013). TDP-43 associates with stalled ribosomes and contributes to cell survival during cellular stress. J. Neurochem. *126*, 288–300.

Ingolia, N.T., Ghaemmaghami, S., Newman, J.R.S., and Weissman, J.S. (2009). Genome-wide analysis in vivo of translation with nucleotide resolution using ribosome profiling. Science *324*, 218–223.

Ingolia, N.T., Lareau, L.F., and Weissman, J.S. (2011). Ribosome profiling of mouse embryonic stem cells reveals the complexity and dynamics of mammalian proteomes. Cell *147*, 789–802.

Ingolia, N.T., Brar, G.A., Rouskin, S., McGeachy, A.M., and Weissman, J.S. (2012). The ribosome profiling strategy for monitoring translation in vivo by deep sequencing of ribosome-protected mRNA fragments. Nat. Protoc. *7*, 1534–1550.

Ingolia, N.T., Brar, G.A., Stern-Ginossar, N., Harris, M.S., Talhouarne, G.J.S., Jackson, S.E., Wills, M.R., and Weissman, J.S. (2014). Ribosome profiling reveals pervasive translation outside of annotated protein-coding genes. Cell Rep. *8*, 1365–1379.

Jan, C.H., Williams, C.C., and Weissman, J.S. (2014). Principles of ER cotranslational translocation revealed by proximity-specific ribosome profiling. Science *346*, 1257521.

Jung, H., Gkogkas, C.G., Sonenberg, N., and Holt, C.E. (2014). Remote control of gene function by local translation. Cell *157*, 26–40.

Juntawong, P., Girke, T., Bazin, J., and Bailey-Serres, J. (2014). Translational dynamics revealed by genome-wide profiling of ribosome footprints in Arabidopsis. Proc. Natl. Acad. Sci. USA *111*, E203–E212.

Kandel, E.R., Dudai, Y., and Mayford, M.R. (2014). The molecular and systems biology of memory. Cell *157*, 163–186.

Kondrashov, N., Pusic, A., Stumpf, C.R., Shimizu, K., Hsieh, A.C., Ishijima, J., Shiroishi, T., and Barna, M. (2011). Ribosome-mediated specificity in Hox mRNA translation and vertebrate tissue patterning. Cell *145*, 383–397.

Kukhanova, M., Streltsov, S., Victorova, L., Azhayev, A., Gottikh, B., and Krayevsky, A. (1979). The donor site of the peptidyltransferase center of ribosomes: equilibrium association constants of model substrates and inhibitors. FEBS Lett. *102*, 198–203.

Lakkaraju, A.K., Abrami, L., Lemmin, T., Blaskovic, S., Kunz, B., Kihara, A., Dal Peraro, M., and van der Goot, F.G. (2012). Palmitoylated calnexin is a key component of the ribosome-translocon complex. EMBO J. *31*, 1823–1835.

Lamberti, A., Caraglia, M., Longo, O., Marra, M., Abbruzzese, A., and Arcari, P. (2004). The translation elongation factor 1A in tumorigenesis, signal transduction and apoptosis: review article. Amino Acids *26*, 443–448.

Lareau, L.F., Hite, D.H., Hogan, G.J., and Brown, P.O. (2014). Distinct stages of the translation elongation cycle revealed by sequencing ribosome-protected mRNA fragments. eLife *3*, e01257.

Lauria, F., Tebaldi, T., Bernabò, P., Groen, E.J.N., Gillingwater, T.H., and Viero, G. (2018). riboWaltz: optimization of ribosome P-site positioning in ribosome profiling data. PLoS Comput. Biol. *14*, e1006169.

Lee, S., Liu, B., Lee, S., Huang, S.-X., Shen, B., and Qian, S.-B. (2012). Global mapping of translation initiation sites in mammalian cells at single-nucleotide resolution. Proc. Natl. Acad. Sci. USA *109*, E2424–E2432.

Li, G.-W., Burkhardt, D., Gross, C., and Weissman, J.S. (2014). Quantifying absolute protein synthesis rates reveals principles underlying allocation of cellular resources. Cell *157*, 624–635.

Liu, B., and Qian, S.-B. (2016). Characterizing inactive ribosomes in translational profiling. Translation (Austin) *4*, e1138018.

Liu, B., Han, Y., and Qian, S.B. (2013). Cotranslational response to proteotoxic stress by elongation pausing of ribosomes. Mol. Cell *49*, 453–463.

Liu, T.-Y., Huang, H.H., Wheeler, D., Xu, Y., Wells, J.A., Song, Y.S., and Wiita, A.P. (2017). Time-resolved proteomics extends ribosome profiling-based measurements of protein synthesis dynamics. Cell Syst. *4*, 636–644.e9.

Martin, K.C., Michael, D., Rose, J.C., Barad, M., Casadio, A., Zhu, H., and Kandel, E.R. (1997). MAP kinase translocates into the nucleus of the presynaptic cell and is required for long-term facilitation in Aplysia. Neuron *18*, 899–912.

McCamphill, P.K., Farah, C.A., Anadolu, M.N., Hoque, S., and Sossin, W.S. (2015). Bidirectional regulation of eEF2 phosphorylation controls synaptic plasticity by decoding neuronal activity patterns. J. Neurosci. *35*, 4403–4417.

Morisaki, T., Lyon, K., DeLuca, K.F., DeLuca, J.G., English, B.P., Zhang, Z., Lavis, L.D., Grimm, J.B., Viswanathan, S., Looger, L.L., et al. (2016). Real-time quantification of single RNA translation dynamics in living cells. Science *352*, 1425–1429.

Nissen, P., Hansen, J., Ban, N., Moore, P.B., and Steitz, T.A. (2000). The structural basis of ribosome activity in peptide bond synthesis. Science *289*, 920–930.

Odom, O.W., Picking, W.D., and Hardesty, B. (1990). Movement of tRNA but not the nascent peptide during peptide bond formation on ribosomes. Biochemistry *29*, 10734–10744.

Ong, S.-E., and Mann, M. (2006). A practical recipe for stable isotope labeling by amino acids in cell culture (SILAC). Nat. Protoc. *1*, 2650–2660.

Pestka, S., Rosenfeld, H., Harris, R., and Hintikka, H. (1972). Studies on transfer ribonucleic acid-ribosome complexes. XXI. Effect of antibiotics on peptidyl-puromycin synthesis by mammalian polyribosomes. J. Biol. Chem. *247*, 6895–6900.

Piccirillo, C.A., Bjur, E., Topisirovic, I., Sonenberg, N., and Larsson, O. (2014). Translational control of immune responses: from transcripts to translatomes. Nat. Immunol. *15*, 503–511.

Pisareva, V.P., Skabkin, M.A., Hellen, C.U., Pestova, T.V., and Pisarev, A.V. (2011). Dissociation by Pelota, Hbs1 and ABCE1 of mammalian vacant 80S ribosomes and stalled elongation complexes. EMBO J. *30*, 1804–1817.

Rivera, C., Saavedra, F., Alvarez, F., Díaz-Celis, C., Ugalde, V., Li, J., Forné, I., Gurard-Levin, Z.A., Almouzni, G., Imhof, A., and Loyola, A. (2015). Methylation of histone H3 lysine 9 occurs during translation. Nucleic Acids Res. *43*, 9097–9106.

Roberts, R.W., and Szostak, J.W. (1997). RNA-peptide fusions for the in vitro selection of peptides and proteins. Proc. Natl. Acad. Sci. USA *94*, 12297–12302.

Schmeing, T.M., Seila, A.C., Hansen, J.L., Freeborn, B., Soukup, J.K., Scaringe, S.A., Strobel, S.A., Moore, P.B., and Steitz, T.A. (2002). A pre-translocational intermediate in protein synthesis observed in crystals of enzymatically active 50S subunits. Nat. Struct. Biol. *9*, 225–230.

Schmidt, E.K., Clavarino, G., Ceppi, M., and Pierre, P. (2009). SUnSET, a nonradioactive method to monitor protein synthesis. Nat. Methods *6*, 275–277.

Schneider-Poetsch, T., Ju, J., Eyler, D.E., Dang, Y., Bhat, S., Merrick, W.C., Green, R., Shen, B., and Liu, J.O. (2010). Inhibition of eukaryotic translation elongation by cycloheximide and lactimidomycin. Nat. Chem. Biol. *6*, 209–217.

Shi, Z., Fujii, K., Kovary, K.M., Genuth, N.R., Röst, H.L., Teruel, M.N., and Barna, M. (2017). Heterogeneous ribosomes preferentially translate distinct subpools of mRNAs genome-wide. Mol. Cell *67*, 71–83.e7.

Stadler, M., Artiles, K., Pak, J., and Fire, A. (2012). Contributions of mRNA abundance, ribosome loading, and post- or peri-translational effects to temporal repression of C. elegans heterochronic miRNA targets. Genome Res. *22*, 2418–2426.

Starck, S.R., Green, H.M., Alberola-Ila, J., and Roberts, R.W. (2004). A general approach to detect protein expression in vivo using fluorescent puromycin conjugates. Chem. Biol. *11*, 999–1008.

Tebaldi, T., Re, A., Viero, G., Pegoretti, I., Passerini, A., Blanzieri, E., and Quattrone, A. (2012). Widespread uncoupling between transcriptome and translatome variations after a stimulus in mammalian cells. BMC Genomics *13*, 220.

Thomas, G., Martin-Pérez, J., Siegmann, M., and Otto, A.M. (1982). The effect of serum, EGF, PGF2 α and insulin on S6 phosphorylation and the initiation of protein and DNA synthesis. Cell *30*, 235–242.

Topisirovic, I., and Sonenberg, N. (2015). Translation and cancer. Biochim. Biophys. Acta *1849*, 751–752.

Viero, G., Lunelli, L., Passerini, A., Bianchini, P., Gilbert, R.J., Bernabò, P., Tebaldi, T., Diaspro, A., Pederzolli, C., and Quattrone, A. (2015). Three distinct ribosome assemblies modulated by translation are the building blocks of polysomes. J. Cell Biol. *208*, 581–596.

Welch, M., Chastang, J., and Yarus, M. (1995). An inhibitor of ribosomal peptidyl transferase using transition-state analogy. Biochemistry *34*, 385–390.

Wilson, D.N. (2014). Ribosome-targeting antibiotics and mechanisms of bacterial resistance. Nat. Rev. Microbiol. *12*, 35–48.

Wu, B., Eliscovich, C., Yoon, Y.J., and Singer, R.H. (2016). Translation dynamics of single mRNAs in live cells and neurons. Science *352*, 1430–1435.

Xue, S., Tian, S., Fujii, K., Kladwang, W., Das, R., and Barna, M. (2015). RNA regulons in Hox 5′ UTRs confer ribosome specificity to gene regulation. Nature *517*, 33–38.

Yarmolinsky, M.B., and Haba, G.L. (1959). Inhibition by puromycin of amino acid incorporation into protein. Proc. Natl. Acad. Sci. USA *45*, 1721–1729.

Yordanova, M.M., Loughran, G., Zhdanov, A.V., Mariotti, M., Kiniry, S.J., O'Connor, P.B.F., Andreev, D.E., Tzani, I., Saffert, P., Michel, A.M., et al. (2018). AMD1 mRNA employs ribosome stalling as a mechanism for molecular memory formation. Nature *553*, 356–360.

STAR★METHODS

KEY RESOURCES TABLE

REAGENT or RESOURCE	SOURCE	IDENTIFIER
Antibodies		
RPS6	Cell Signaling	AB_331355
RPL26	Abcam	AB_945306
eIF4B	Abcam	AB_11156354
eIF4A1	Abcam	AB_732122
PABP	Abcam	AB_777008
hb-EGF	Abcam	N/A
CYP27A1	Abcam	AB_11128459
H3	Abcam	AB_302613
eEF2	Abcam	AB_732081
RPL14	Abcam	N/A
Pelo	Abcam	N/A
COX4	Abcam	AB_2616599
PLK3	Thermo Scientific	AB_2167750
PALLD	Thermo Scientific	AB_1115217
Calnexin	Millipore	AB_2069152
H3(K9)H3	Millipore	AB_310625
EGFP	Roche	N/A
Actin	Santa Cruz	AB_1119529
Streptavidin-HRP	Promega	N/A
Chemicals, Peptides, and Recombinant Proteins		
Cycloheximide	Sigma	01810
Tizol	Sigma	T9424
SUPERase In RNase Inhibitor	Life Technologies	AM2696
Epithelial Growth Factor	RD System	236E4
Ribo-Zero rRNA Removal Kit	Illumina	MRZH11124
Small RNA chip	Agilent	067-1548
Luciferase SP6 control DNA	Promega	L4741
pGEMEX-1	Promega	P2211
D-Biotin	Sigma	B4501
N-hydroxysuccinimide	Pierce	HC102040
DMF	Sigma	27056
N,N'-Dicyclohexylcarbodiimide	Sigma	D80002
CDI	Sigma	21860
BOC anhydride	Sigma	361941
Puromycin	Sigma	P8833
Trifluoroacetic acid	Sigma	302031
Stationary phase RP18	Phenomenex Kinetex	00G-4601-E0
Dynabeads® MyOne Streptavidin C1	Life Technology	65001
Critical Commercial Assays		
TnT Quick Coupled Transcription/Translation System	Promega	#L2881
Deposited Data		
Sequencing data (mouse brain)	This study	GEO: GSE102354
Sequencing data (HEK293)	This study	GEO: GSE112353

(*Continued on next page*)

Continued

REAGENT or RESOURCE	SOURCE	IDENTIFIER
Sequencing data (MCF7)	This study	GEO: GSE112295
Proteomics data (MCF7)	This study	ProteomeXchange: PXD009417
Ribosome profiling data (mouse brain)	Lauria et al., 2018	GEO: GSE102318
Reference mouse genome annotation Gencode M6	Gencode	https://www.gencodegenes.org/mouse_releases/6.html
Reference human genome annotation Gencode 25	Gencode	https://www.gencodegenes.org/releases/25.html
Experimental Models: Cell Lines		
MCF7	ATCC	ATCC® HTB-22
NSC34	CEDARLANE	CLU140
HeLa	N/A	N/A
HEK293	N/A	N/A
Experimental Models: Organisms/Strains		
Wild-type mice	University of Edinburgh, Tom Gillingwater Lab	N/A
Oligonucleotides		
qPCR primers for IVTT	this paper	See Table S1
Primes for ribosome profiling	Ingolia et al., 2012 and Illumina (Epicenter)	See Table S2 and ARTseq Ribosome Profiling Kit (RPHMR12126)
Taqman probes	Thermo Fisher Scientific	See Table S3
Software and Algorithms		
riboWaltz v1.0.0	Lauria et al., 2018	https://github.com/LabTranslationalArchitectomics/riboWaltz
Tophat v2.0.14	https://ccb.jhu.edu/software/tophat/index.shtml	N/A
R v3.3.0	https://www.r-project.org/	N/A
Bioconductor v3.3	https://www.bioconductor.org/	N/A
Cufflinks v2.2.1	https://github.com/cole-trapnell-lab/cufflinks	N/A
Trimmomatic v0.36	http://www.usadellab.org/cms/?page=trimmomatic	N/A
Bowtie2 v2.2.6	http://bowtie-bio.sourceforge.net/bowtie2/index.shtml	N/A
enrichR	http://amp.pharm.mssm.edu/Enrichr/	N/A
MaxQuant v1.6.1.0	http://www.biochem.mpg.de/5111795/maxquant	N/A

CONTACT FOR REAGENT AND RESOURCE SHARING

Further information and requests for resources and reagents should be directed to and will be fulfilled by the Lead Contact, Gabriella Viero (gabriella.viero@cnr.it).

EXPERIMENTAL MODEL AND SUBJECT DETAILS

Tissues, cell lines and growth conditions

Human MCF7 (ATCC catalog no. ATCC® HTB-22), HeLa cells and HEK293 cells and murine NSC34 (CEDARLANE catalog no. CLU140) cell lines were seeded on adherent plates and maintained at 37°C, 5% CO_2 in DMEM supplemented with 10% Fetal Bovine Serum (FBS), 2 mM L-glutamine, 100 units/mL penicillin and 100 μg/mL of streptomycin. Cells were used at 80% of confluence. For starvation treatments cells were kept 0.5% FBS, 2 mM L-glutamine, 100 units/mL penicillin and 100 μg/mL of streptomycin for at least 12. For EGF treatment, after starvation EFG was added at 1 μg/mL for 4 h.

Wild-type mice mice were obtained from breeding stocks at the University of Edinburgh. All procedures were performed under licensed authority from the UK Home Office (PPL 60/4569).

METHOD DETAILS

Chemical synthesis of the 3P molecule

A solution of DCC in DMF was added dropwise to Biotin and NHS in DMF, to obtain a white precipitate (Biotin-NHS). Biotin-NHS in MeCN was added to a jeffamine (2,2'-(Ethylenedioxy)bis(ethylamine) - MeCN solution to yield a white hygroscopic solid (BJ1), then dissolved in dry pyridine and reacted with CDI to obtain a product called BJ1′. Puromycin was dissolved in pyridine, reacted with CDI and added to a BOC protected jeffamine in DCM. The product (PJ) was partitioned between DCM and water, evaporated and triturated in ethyl acetate. Trifluoroacetic acid was added dropwise to a stirred suspension of PJ in DCM. The solution was cooled and stirred overnight, diluted with chloroform and the solvent evaporated to give a yellow oil product (PJ′). BJ1′ and PJ′ were dissolved in pyridine and stirred overnight under N2. The product (3P) was purified by column chromatography and preparative HPLC.

Depletion assay of 3P with streptavidin coated beads

A volume of 50 μL of 2 M NaCl, 1 mM 3P, 1 mM EDTA, 10 mM Tris-HCl, pH 7.5 in DEPC water, was added to different amount of magnetic beads and the suspension was incubated for 5 min at RT. After separation on a magnetic rack, the absorbance of the supernatant was measured at 272 nm.

In vitro - cell free Transcription/Translation

In vitro translation reactions of the full-length Luciferase (inserted in SP6 DNA plasmid, Promega) and full-length EGFP (inserted in the IP-PR2 plasmid) were obtained with the TnT Quick Coupled Transcription/Translation System (Promega) according to manufacturer's instructions.

Preparation of RiboLace beads

For each sample, a volume of 20 μL of Dynabeads® MyOne Streptavidin C1 (Life Technology) or 30 μL of Streptavidin Mag Sepharose (10% slurry, GE Healthcare Life Sciences) were washed for 5 min with a 0.05 M NaCl, 0.1 M NaOH, in DEPC-treated water. Then, beads were washed with 500 μL of nuclease free water and with Binding Buffer (2 M NaCl, 10 mM Tris-HCl, pH 7.5 in DEPC water). For functionalization with 3P, 30 μL of a 1 mM solution of 3P in Binding Buffer was added to the beads followed by an incubation of 1 h, mixing at 1400 rpm at 20°C. Beads were end-capped by incubating for 10 min at 1400 rpm at RT in the presence of biotin-methoxypolyethylene glycol conjugate (mP, Creative Pegworks) at 0.5 mM. RiboLace beads were washed with 500 μL of nuclease free water, placed on a magnet for 2 min, and washed with 500 μL of nuclease free water. The efficiency of binding was calculated by measuring the ratio between the absorbance of the supernatant at 270 nm, and the absorbance at 270nm of a 1 mM starting solution. Finally, beads were washed twice with 500 μL of W-buffer (10 mM NaCl, 10 mM $MgCl_2$, 20 μg/mL cycloheximide, 10 mM HEPES, pH 7 in DEPC water) and used for active ribosome pull-down. As a negative control, beads were functionalized with a 0.5 mM solution of a biotin-methoxypolyethylene glycol conjugate (1000 Daltons, Creative Pegworks).

RiboLace and IVTT system

IVTT mix reaction (Promega) was used with the abovementioned plasmids for 40 min. The reaction was stopped adding cycloheximide (10 μg/mL) for 3 minutes before addition of W-buffer. The solution was divided into 3 vials, each containing 150 μL. The first was used for the extraction of total RNA, the second used with RiboLace, and the third for control mP-beads. For RiboLace, the reaction mix was added to the functionalized beads and incubated for 1 h in orbital rotation at 2 rpm at 4°C. The tube was then kept on ice on a magnetic stand for 5 min to pellet the beads–bounded-ribosomes. The supernatant was separated and beads washed two times with 500 μL of W-buffer. Beads were dissolved in 100 μL of 100 mM NaCl, 10 mM MgCl2, Trizma HCL, pH 7.5 in DEPC water. RNA was extracted from the beads–bounded-ribosomes with Trizol (Thermo Fischer Scientific) and solubilized in 30 μL of RNase-free water and DNase I treated. cDNA was obtained synthesis and RT-qPCR were run using KAPA SYBT FAST qPCR kit (KAPA Biosystem) according to the following protocol: 3 min - 95°C activation; 2 s - 95°C, 20 s – 57°C; 25 cycles; 65°C to 95°C melting ramp. Primers are listed in Table S1. Data were processed with Bio-Rad CFX-Manager 1.6 software. The fold change ratio was determined as the ratio between the ΔΔCt of treated and not treated sample. The delta cross-threshold (ΔCt) was determined respect to the total RNA and the relative ΔΔCt calculated respect to the control (mP-beads ΔCt).

For determining the total amount of newly synthesized proteins, we employed ε-labeled biotinylated lysine-tRNA complex using Transcend Non-Radioactive Translation Detection Systems according to the manufacturer's instructions (Promega) and the effective translation verified by SDS–PAGE.

Luciferase assay

Real-time measurements of luciferase activity were recorded at 37°C with 5% CO_2 using the Infinite 200 PRO reader (Tecan), according to manufacturer's instructions. In brief, the IVTT reactions were plated in a 96-well plate and the luciferase translation efficiency was monitored by means of luminescence signal using the Bright-Glo Luciferase Assay System (Promega).

Purification of active polysomes and ribosomes with RiboLace

MCF7, HeLa, HEK293 or NSC-34 cells were seeded at 1.5 × 10^6 cells/dish and kept in culture until reaching 80% of confluence. Cells were then treated with 10 μg/mL of cycloheximide (CHX) for 5 min at 37°C before lysis. Cell lysates were obtained according to (Viero et al., 2015). Tissues were dissected immediately following sacrifice and pulverized under liquid nitrogen using a pestle and a mortar and the lysates was obtained according to (Bernabò et al., 2017), The lysate was aliquoted and stored at −80°C for not more than a month, avoiding more than one freeze/thaw cycle.

RNA absorbance was measured (260 nm) by Nanodrop ND-1000 UV-VIS Spectrophotometer and the lysate diluted to 0.5 - 1.7 a.u. A260/μL with W-buffer (10 mM NaCl, 10 mM $MgCl_2$, 20 μg/mL cycloheximide, 10 mM HEPES, pH 7 in DEPC water). For polysome profiling with RiboLace, the solution obtained was added directly to the functionalized beads and the suspension incubated on a wheel for 1 hour in orbital rotation, 3 rpm (StarLab Rotator), at 4°C. The tube was then kept on ice on a magnetic stand for 5 min to pellet the beads–bounded-ribosomes and washed twice with W-buffer. RNA was extracted by acidic-phenol chloroform separation. The quality of the RNA samples was assessed using Agilent Bioanalyzer 2100 and Nanodrop ND-1000 Spectrophotometer (Thermo Scientific). Whole transcriptome library preparation was performed starting from 1 μg of total RNA with RIN ≥ 8. Following enrichment of poly-A containing mRNA molecules using poly-dT oligo-attached magnetic beads, all recovered RNA was processed using the Illumina TruSeq RNA Sample Preparation Kit sequenced. Sequencing was carried out on Illumina HiSeq 2000 using the protocol HCS 1.5.15.1 in single reads.

For ribosome profiling with RiboLace, a total volume of lysate corresponding to 0.3 $A.U._{260nm}$ was treated with 1.5 U of Artseq nuclease (Epicenter) or RNaseI for 45 min at 20°C. The reaction was stopped with 10U SUPERase In RNase inhibitor, 10 min on ice. Then, the sample was incubated with RiboLace beads for 1 hour in orbital rotation, 3 rpm (StarLab Rotator) at 4°C. The tubes were then kept on ice on a magnetic stand for 5 min to pellet the beads–bounded-ribosomes. The supernatant was discarded (unbound fraction) and beads washed twice with W-buffer. Finally, beads were solubilized in 200 μL of W buffer containing 20 U SUPERase In. The RNA was extracted using acid-phenol:chloroform (Ambion) after incubation with 1% SDS, 0.1 mg of proteinase K (Euroclone) at 37°C for 75 min. Library preparation was adapted from a previous protocol (Ingolia et al., 2012). The ribosome profiling library PCR forward primer and indexed reverse primers are in Table S2. Libraries (175 nt) were PAGE purified from a 8% not-denaturing TBE polyacrylamide and characterized using the Agilent 2100 Bioanalyzer (High-Sensitivity DNA assay).

Ribo-Seq data were obtained using the protocol in (Ingolia et al., 2012).

RNA extraction for RNA-Seq and POL-Seq

For RNA-Seq the RNA was extracted from MCF7 cell lysates, obtained as previously described, with acid phenol:chloroform (Ambion catalog no. AM9720) extraction. For total polysomal RNA extraction, polysomes were obtained according to (Viero et al., 2015) using sucrose gradient fractionation. Briefly, sucrose fractions were collected and treated with 200 μg/mL proteinase K (Life technologies), 1% SDS in DEPC water and RNase Inhibitor (0.4 a.u./μL) for 1.5 h at 37°C. After phenol:chloroform extraction and isopropanol precipitation, polysomal RNA was quantified by Nanodrop ND-1000 UV-VIS Spectrophotometer and Agilent 2100 Bioanalyzer with RNA 6000 pico kit (Agilent).

Whole transcriptome library preparation was performed starting from 1 μg of total RNA with RIN ≥ 8. Following enrichment of poly-A containing mRNA molecules using poly-dT oligo-attached magnetic beads, all recovered RNA was processed using the Illumina TruSeq RNA Sample Preparation Kit (Illumina #FC-122-1001 #FC-122-1002) and the protocol v2 Rev. C. Completed libraries were evaluated by DNA quantification and Bioanalyzer analysis (mean fragment length = 274 bp), and then submitted for sequencing. RNA-seq was constructed with barcodes to allow multiplexing of 12 samples per lane. Sequencing was carried out on Illumina HiSeq 2000 using the protocol HCS 1.5.15.1 in single reads. Experiments were performed in biological duplicate.

Immunoblotting

Cell lysates were prepared in hypotonic lysis buffer (10 mM NaCl, 10 mM $MgCl_2$, 10 mM Tris–HCl, pH 7.5, 1% Triton X-100, 1% sodium deoxycholate, 5 U/mL DNaseI, 200 U/mL RNase inhibitor, 1 mM dithiothreitol and 10 μg/mL cycloheximide) or RIPA buffer. Proteins were separated in SDS–polyacrylamide gel electrophoresis and transferred onto PVDF membranes. The membranes were blocked in 5% BSA (Sigma) in TBS-Tween (0.1% Tween) for 1 hour, incubated in primary antibody o.n. The primary antibodies used are listed in the STAR Methods section. After incubation with secondary antibodies conjugated to horseradish peroxidase and extensive washing, the blots were developed using ECL Plus (GE Healthcare,) or SuperSignal West Femto Maximum Sensitivity Substrate (Thermo Scientific). Signals were acquired with ChemDoc-It (Bio-Rad) and analyzed with ImageJ software (v 1.45 s). All experiments were run in triplicate.

qPCR

RNA expression was analyzed by TaqMan assay, the gene name, aliases, chromosome location and TaqMan ID are reported in Table S3. All TaqMan probes were purchased from Life Technologies. Relative quantification of target genes was determined calculating the delta cross-threshold (ΔCt) respect to the 18S housekeeping gene and the relative ΔΔCt calculated respect to the total RNA sample, according to the Pfaffl method. RT was performed using random hexamers, single strand reverse transcriptase (RevertAid RT Reverse Transcription Kit, Life Technologies #K1622).

Protein sample preparation for MS

MCF7 cells were grown in 100 mm Petri dishes in complete medium (10% FBS) or under starvation (1% FBK) for 12 h. Two dishes were lysed with RIPA buffer (50mM Tris pH 7.4, 150mM NaCl, 0.25% Igepal, 1mM EDTA and 0.5% Sodium Deoxycholate) in the presence of 0.5% Phosphatase Inhibitor Cocktails, 5 μg/mL Peptastin A and 0.25% Protease Inhibitor Cocktail. After protein extraction according to the methanol-chloroform procedure, proteins were solubilized in 6 M urea/2 M thiourea, 10 mM HEPES pH 8.0 and incubated at RT for 30min in the presence of 5mM DTT and for additional 20min with 5.5mM iodoacetamide. Peptides were obtained by digestion with 1μg of LysC solution/50μg of protein for 3 hours at RT and then with 1μg of Trypsin/50μg protein overnight. Peptides were purified on C18 Pipette Tips (Pierce, Thermo Scientific). Mass spectra were acquired in the Orbitrap Fusion Tribrid analyzer at Thermo Fisher Scientific, Switzerland. Experiments were performed in triplicates.

QUANTIFICATION AND STATISTICAL ANALYSIS

Data analysis of RNA-seq and POL-seq experiments

Fastq files were checked for quality control with FastQC. Reads generated from each sample were aligned to the human genome with Tophat (version 2.0.14), using the Gencode 22 transcript annotation as transcriptome guide. All programs were used with default settings. Mapped reads were assembled into transcripts guided by reference annotation (Gencode 22) with Cufflinks (version 2.2.1). Expression levels were quantified by Cufflinks with normalized FPKM (fragments per kilobase of exon per million mapped fragments). Differential expression analysis was performed with Cuffdiff.

Data analysis of MS

The raw MS data were analyzed with MaxQuant software version 1.6.1.0 using default settings and Label Free Quantification (LFQ).

Data analysis of ribosome profiling experiments

For all ribosome profiling analyses we used riboWaltz (Lauria et al., 2018). Briefly, reads were processed by removing 5' adapters, discarding reads shorter than 20 nucleotides and trimming the first nucleotide of the remaining ones (using Trimmomatic v0.36). For the mouse brain and the HEK293 dataset, respectively, reads mapping on the collection of *M. musculus* and *H. sapiens* rRNAs (from the SILVA rRNA database, release 119) and tRNAs (from the Genomic tRNA database: gtrnadb.ucsc.edu/) were removed. Remaining reads were mapped on the mouse transcriptome (using the Gencode M6 transcript annotations) or human transcriptome (Gencode 25): antisense reads were removed and reads entirely mapping to the same nucleotides were considered identical and collapsed. All the alignments were performed with Bowtie2 (v2.2.6) employing default settings. Normalization among replicates was performed with the trimmed mean of M-values normalization method (TMM) implemented in edgeR. Protein coding transcripts used for further analyses were selected using a threshold on their signal (FPKM and CPM values > 80^{th} percentile). Differential analyses between RiboLace and Ribo-Seq were performed with the edgeR Bioconductor package. Significantly enriched transcripts were selected with the following thresholds: absolute log2 fold enrichment > 1, P value < 0.05, normalized number of ribosome-protected fragment > 1 per million. Functional annotation enrichment analyses were performed with Enrichr (http://amp.pharm.mssm.edu/Enrichr/).

DATA AND SOFTWARE AVAILABILITY

Raw and analyzed sequencing data have been deposited under GEO: GSE102354 (mouse brain), GSE112353 (HEK293), GSE112295 (MCF7). The mass spectrometry proteomics data have been deposited to the ProteomeXchange Consortium (http://proteomecentral.proteomexchange.org) via the PRIDE partner repository with the dataset identifier PXD009417. Classic ribosome profiling (Ribo-Seq) data from mouse brain were retrieved from GEO: GSE102318.